Cell Chemical Biology

# RAMIHM generates fully human monoclonal antibodies by rapid mRNA immunization of humanized mice and BCR-seq

## Graphical abstract

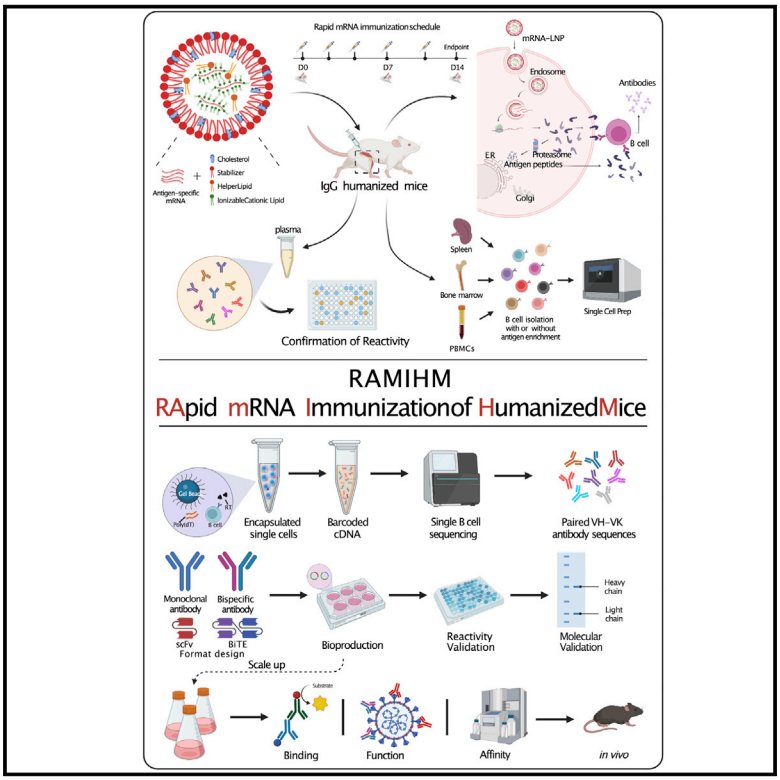


## Highlights

- RAMIHM is an efficient strategy to rapidly generate fully human monoclonal antibodies
- RAMIHM generates human SARS-CoV-2 antibodies against multiple Omicron sublineages
- RAMIHM is applicable to cancer and immunology targets such as CD22 and GPRC5D

## Authors

Ping Ren, Lei Peng, Luojia Yang, ..., Paul Clark, Daryl Klein, Sidi Chen

## Correspondence

sidi.chen@yale.edu

## In brief

Ren et al. develop a highly efficient strategy (RAMIHM) to generate fully human mAbs and apply it to generate several potent and specific SARS-CoV-2 neutralizing monoclonal antibodies against six Omicron sublineages. RAMIHM also demonstrates applicability to cancer and immunology targets such as CD22 and GPRC5D.

Ren et al., 2023, Cell Chemical Biology *30*, 85–96
January 19, 2023 
https://doi.org/10.1016/j.chembiol.2022.12.005

CellPress

Cell Chemical Biology

CellPress

Resource

# RAMIHM generates fully human monoclonal antibodies by rapid mRNA immunization of humanized mice and BCR-seq

Ping Ren,[1,2,3,11] Lei Peng,[1,2,3,11] Luojia Yang,[1,2,3] Kazushi Suzuki,[1,2,3] Zhenhao Fang,[1,2,3] Paul A. Renauer,[1,2,3,4] Qianqian Lin,[1,2,3] Meizhu Bai,[1,2,3] Tongqing Li,[6,7] Paul Clark,[1,2,3] Daryl Klein,[6,7] and Sidi Chen[1,2,3,4,5,8,9,10,12,*]
[1]Department of Genetics, Yale University School of Medicine, New Haven, CT 06520, USA
[2]System Biology Institute, Yale University, West Haven, CT 06520, USA
[3]Center for Cancer Systems Biology, Yale University, West Haven, CT 06520, USA
[4]Molecular Cell Biology, Genetics, and Development Program, Yale University, New Haven, CT 06520, USA
[5]Immunobiology Program, Yale University, New Haven, CT 06520, USA
[6]Department of Pharmacology, Yale University, New Haven, CT 06520, USA
[7]Cancer Biology Institute, Yale University, New Haven, CT 06520, USA
[8]Comprehensive Cancer Center, Yale University School of Medicine, New Haven, CT 06520, USA
[9]Stem Cell Center, Yale University School of Medicine, New Haven, CT 06520, USA
[10]Center for Biomedical Data Science, Yale University School of Medicine, New Haven, CT 06520, USA
[11]These authors contributed equally
[12]Lead contact
*Correspondence: sidi.chen@yale.edu
https://doi.org/10.1016/j.chembiol.2022.12.005

## SUMMARY

As a clinical vaccine, lipid nanoparticle (LNP) mRNA has demonstrated potent and broad antibody responses, leading to speculation about its potential for antibody discovery. Here, we developed RAMIHM, a highly efficient strategy for developing fully human monoclonal antibodies that employs rapid mRNA immunization of humanized mice followed by single B cell sequencing (scBCR-seq). We immunized humanized transgenic mice with RAMIHM and generated 15 top-ranked clones from peripheral blood, plasma B, and memory B cell populations, demonstrating a high rate of antigen-specificity (93.3%). Two Omicron-specific neutralizing antibodies with high potency and one broad-spectrum neutralizing antibody were discovered. Furthermore, we extended the application of RAMIHM to cancer immunotherapy targets, including a single transmembrane protein CD22 and a multi-transmembrane G protein-coupled receptor target, GPRC5D, which is difficult for traditional protein immunization methods. RAMIHM-scBCR-seq is a broadly applicable platform for the rapid and efficient development of fully human monoclonal antibodies against an assortment of targets.

## INTRODUCTION

Monoclonal antibodies (mAbs) are widely used as predominant therapeutics for diverse diseases, offering exquisite specificity and affinity for specific targets on both cell-surface and secreted proteins. Since the FDA approved the first clinical mAb in the 1970s, over 100 mAbs have been approved by the agency, with the majority targeting soluble proteins and single transmembrane proteins.[1] Although certain soluble/single-transmembrane proteins have been successfully used in antibody-based therapies, there are a very limited number of such proteins. Consequently, it is imperative to explore complex multi-transmembrane protein families, including ion channels and G protein-coupled receptors (GPCRs), which are among the most commonly exploited therapeutic targets, contributing over a third of the FDA approvals.[2–5] Significant features of approved GPCR-modulating drugs are nearly all small molecules or peptides, and only two GPCR mAbs to date have been approved by the FDA, namely erenumab and mogamulizumab.[6,7]

Moreover, viral transmembrane proteins have become important anti-viral therapeutic targets since the emergence of COVID-19. The spike protein of COVID-19 pathogen SARS-CoV-2 displays high mutation rates, and each mutation can affect functional properties or alter infectivity. Several ''variants of concern'' (VoCs) of SARS-CoV-2 have emerged during the past 3 years and have led to continuous waves of pandemic due to spike mutations that enhance virus transmissibility, antigenicity, and immune evasion. The Omicron variant is one of the most recent SARS-CoV-2 variants, containing over 30 mutations and deletions in its spike protein, including 17 within the receptor binding domain (RBD) compared with ancestral SARS-CoV-2 variants. A number of studies have proven that

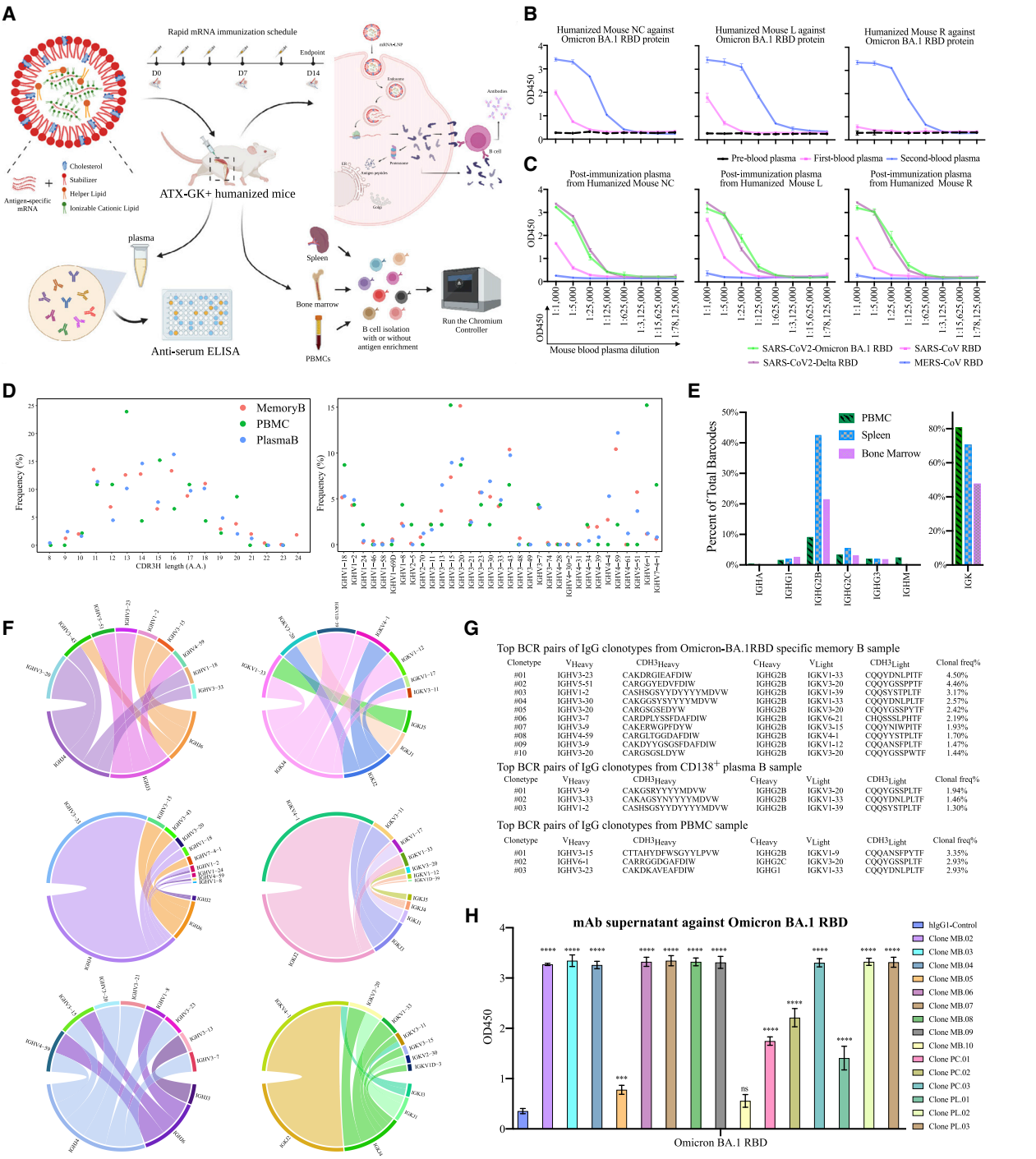


**Figure 1. Evaluation of Omicron BA.1-RAMIHM humanized mice and rapid characterization of fully human Omicron BA.1-specific monoclonal antibodies**

(A) Schematic illustration of the humoral immune responses induced by RAMIHM and antibody discovery. Three humanized mice were repeatedly immunized with Omicron LNP-mRNA as an immunogen. 10 μg of Omicron LNP-mRNA was given to each mouse on day 0, day 2, day 4, and day 7, followed by 20 μg of Omicron LNP-mRNA injected on day 11. Retro-orbital blood was collected on day 0, day 7, and day 14. Plasma was isolated from the blood for downstream experiments. Spleen, bone marrow, and PBMCs were collected for downstream antibody library preparation, and antibody sequences were characterized by single B cell sequencing.

(B) Antibody titer determination in plasma samples. The Omicron BA.1RAMIHA immunized mice were defined as Mouse NC (no ear clipping), Mouse L (left ear clipping), and Mouse R (right ear clipping) based on ear clipping. All plasma samples were serially 5-fold diluted from 1:1000 and assayed by a direct-coating ELISA with Omicron BA.1 RBD protein-coated plate. Error bars represent the mean ± SEM of triplicates with individual data points in plots.

*(legend continued on next page)*

the early BA.1 sublineage of Omicron renders most previously authorized monoclonal antibodies ineffective,[8,9] causing them to be no longer recommended in the COVID-19 treatment guidelines for patients with Omicron infections. Despite widespread vaccinations, certain populations are still vulnerable to the diseases, and hospitalizations and deaths still occur daily due to a high rate of breakthrough infections and frequent reinfections in the high-risk populations. As a consequence, rapidly developing next-generation antibodies that retain potency against Omicron are required when the effectiveness of current vaccines and approved antibody therapies is threatened.[10]

In this study, we present a platform for monoclonal antibody discovery named RApid mRNA Immunization of Humanized Mice (RAMIHM), a highly efficient strategy that utilizes rapid mRNA immunization of humanized mice followed by single B cell sequencing (scBCR-seq) to allow efficient development of fully human monoclonal antibodies. The RAMIHM involves the use of high doses of antigen-specific liquid nanoparticle (LNP)-mRNA vaccines to frequently immunize immunoglobulin (Ig) humanized mice in 2 weeks, allowing isolation of antigen-specific high-affinity monoclonal antibodies. Customized scBCR-seq is performed on these immunized mice to acquire the paired human variable region sequences from enriched B cell clonotypes, to allow immediate recombinant generation of potent and specific fully human antibodies. To rapidly demonstrate the RAMIHM as a proof of principle, we directly performed the RAMIHM with Omicron BA.1 spike-encapsulated LNP-mRNA vaccines,[11] combined with the use of customized scBCR-seq to obtain the human variable region sequences from Omicron BA.1 RBD enriched B cell clonotypes. To explore the rapid development of mAbs for cancer immunotherapy, we further employed RAMIHM on current clinical cancer targets. We generated human CD22 full-length-encapsulated LNP-mRNA and RAMIHM with scBCR-seq to obtain the human variable region sequences from human CD22-extracellular domain (ECD) enriched B cell clonotypes. To extend the applicability of RAMIHM on challenging cancer targets such as GPCRs,[12] we applied RAMIHM on GPRC5D to identify the paired human variable region sequences from IgG isotype-positive B cell clonotypes.

## RESULTS

### Development of rapid mRNA immunization of humanized mice, a highly efficient strategy to identify fully human monoclonal antibodies

To date, a two-dose SARS-CoV-2 mRNA-based vaccination strategy has been demonstrated to effectively induce humoral and cellular immunity to SARS-CoV-2, including the ancestral virus (ancestral, reference, wild-type, Wuhan-1, or WA-1, identical sequences) and its VoCs such as the Delta variant.[13,14] However, several recent studies demonstrated that the Omicron BA.1 subvariant has substantial changes in its genome, especially the spike protein (Figure S1A) and illustrated dramatically decreased neutralizing titers in convalescent or vaccinated recipients, causing waning immunity and massive breakthrough infections.[15–18] Importantly, nearly all antibodies initially developed against the ancestral virus have substantially dropped, or completely lost, the neutralization ability against Omicron.[8,19–21] Therefore, next-generation neutralizing antibodies are needed quickly. To combat the rapidly evolving VoCs, we thus developed an antibody discovery approach named RAMIHM, with repetitive intramuscular injections using high doses of LNP-mRNA, followed by B cell isolation, antigen enrichment, and single B cell sequencing (Figure 1A). We applied this directly with Omicron BA.1-spike-encoding LNP-mRNA to induce Omicron-specific immune responses for isolation of Omicron BA.1-targeting mAbs.

Using Omicron BA.1-specific LNP-mRNAs that contain LNP-formulated mRNA encoding the HexaPro engineered full length of Omicron BA.1 spike glycoprotein (STAR Methods), we first characterized the biophysical integrity of these LNP-mRNAs (Figures S1B and S1C) and validated the expression of functional Omicron BA.1 spike protein surface expression via human ACE2 (hACE2) staining of LNP-mRNA transfected HEK293 cells (Figure S1D). Next, we performed the administration of four 10-μg doses and one 20-μg dose of Omicron BA.1-specific mRNA LNP in three IgG-humanized mice and collected retro-orbital blood samples from each humanized mouse before and after booster immunization. Blood samples were labeled as pre-, first, or second immunization draw depending on the

(C) Antibody cross-reactivity measurement. All post-immunized plasma samples (second blood) were serially 5-fold diluted from 1:1000 and assayed by a direct-coating ELISA with a selected pan-CoV-RBD proteins-coated plate. Error bars represent the mean ± SEM of triplicates with individual data points in plots.
(D) B cell characterization by customized scBCR-seq profiling. Left panel, distribution of heavy chain complementarity-determining region 3 (HCDR3) length in each B cell group (Memory B, Plasma B, and PBMC) from Omicron BA.1-RAMIHM mice. Right panel, distributions of heavy chain V-segment in each B cell group (Memory B, Plasma B, and PBMC) from Omicron BA.1-RAMIHM mice. Total number of single cells sequenced with BCRs (Memory B library, n = 2,646; Plasma B library, n = 617; PBMC library, n = 239; total n = 3,502).
(E) Ig class distributions of Omicron BA.1-RAMIHM mice's clonotypes. Distribution and frequency analysis of immunoglobulin isotypes usage in the spleen, bone marrow, and PBMC from Omicron BA.1-RAMIHM mice.
(F) Distribution of top 10 heavy- and light-chain V/J segment recombination. Chord diagrams (circos plots) showing the distribution of top 10 heavy- and light-chain V and J gene-segment recombination obtained in each representative library. Interconnecting lines indicate the relationship between antibodies that share V and J gene segments at both IGH and IGL. Top to bottom: Memory B library, PBMC library, and Plasma B library.
(G) Single B cell variable chains for antibody cloning. Variable (V) genes and CDR3 lengths for paired heavy and light chains of top enriched clones to SARS-CoV-2 Omicron BA.1 from single BCR sequencing.
(H) ELISA of mAbs supernatant binding specificity against Omicron BA.1 RBD protein. All full-length mAb clones from single BCR sequencing and control were evaluated against Omicron BA.1 RBD protein coated on the ELISA plate, and binding activity was recorded at an optical density (OD) of 450 nm. Triplicate data points (n = 3 each). In this figure: data are shown as mean ± SEM plus individual data points in dot plots. Statistics: one-way ANOVA was used to assess statistical significance. Each mAb clone was compared with the control. Multiple testing correction was made to correct the p values. Two-sided tests were performed. The p values are indicated in the plots. Statistical significance labels: *$p < 0.05$; **$p < 0.01$; ***$p < 0.001$; ****$p < 0.0001$. Non-significant comparisons are not shown unless otherwise noted as n.s., not significant. Source data and additional statistics for experiments are in supplemental excel file(s). See also Figures S1–S3 and S7.

collection sequence (Figure 1B). Antibody titers were measured using serial plasma dilutions on ELISA plates coated with recombinant Omicron BA.1 RBD protein. Binding activity was visualized using anti-mouse IgG antibodies at 450-nm optical density (OD). Three sequential plasma samples showed increasing vaccine-elicited antibody responses during each blood collection (Figures 1B and S1D). All post-immunized plasma samples (second blood) exhibited significant reactivity to the recombinant SARS-CoV-2 Omicron BA.1 RBD protein (Figure 1C). In addition, all these samples also showed strong cross-reactivity to recombinant SARS-CoV-2 Delta RBD protein and intermediately cross-reactivity to recombinant SARS-CoV RBD protein but no cross-binding to recombinant MERS-CoV RBD protein (Figure 1C). Together, these results demonstrated Omicron BA.1-specific rapid mRNA immunization (Omicron BA.1-RAMIHM), which also contains broader reactive antibodies against other variant and coronavirus species such as SARS-CoV-2 Delta and SARS-CoV, elicited strong anti-Omicron plasma in all IgG-humanized mice within 2 weeks.

## Customized single-cell BCR sequencing mapped the IgG clonal repertoires of Omicron BA.1-RAMIHM animals

To obtain Omicron BA.1 RBD-specific B cells, we collected them from spleen, lymph nodes, bone marrow, and whole blood from an Omicron BA.1-RAMIHM mouse, and we collected three different types of B cells (memory B cells, plasma B cells, and peripheral blood mononuclear cells) by using different isolation procedures (STAR Methods) for B cell repertoire mapping and reactive BCR identification via scBCR-seq. To prepare the memory B cells enriched library, we enriched memory B cells by immunomagnetic negative selection and used 25 μg of recombinant Omicron BA.1 RBD proteins as bait to obtain Omicron BA.1 RBD-specific memory B cells from pre-enriched memory B cells (Memory B library). To generate a plasma B cell enriched library, we applied an anti-mouse $CD138^+$ plasma cell isolation kit to isolate $CD138^+$ plasma B cells from freshly isolated raw bone marrow cells (Plasma B library). To generate a peripheral blood mononuclear cells library, we isolated peripheral blood mononuclear cells (PBMCs) from whole blood by centrifugation following the PBMC isolation method (PBMC/Peripheral B library). Subsequently, we counted and subjected 10,000 fresh cells from above each B cell for single-cell BCR library preparation and sequencing, respectively. After sequencing, we analyzed 3,502 Omicron BA.1 RBD-specific B cells, and we eventually obtained 2,558 paired antibody sequences. To further decipher Omicron BA.1 RAMIHM-elicited B cell clonal expansion on a single-cell level, we first characterized the dominant B cell clonotypes based on the number of cells observed and frequencies of identical CDR3 region for both heavy and light chains in pairs. By analyzing the BCR repertoires, we mapped the landscape of BCR populations in Memory B, Plasma B, and Peripheral B/PBMC from the Omicron BA.1-RAMIHM immunized mouse (Figure S2, Dataset S1, supplemental codes).

The Omicron BA.1 RBD-specific antibodies had a relative enrichment for IGVH3-7, IGVH3-15, IGVH3-20, IGVH3-23, IGVH3-30, IGVH3-33, IGHV3-43, and IGVH4-59, analyzed from three individual BCR libraries (Figure 1D, Dataset S1). A range of lengths between 8 and 24 aa was observed for these BCR CDRH3s (Figure 1D, Dataset S1). Interestingly, a large portion of IgG2B-expressing B cells was identified from three B cell type isolations (Figure 1E), a signature of potential involvement of Th2 cells in B cells maturation and class switch in these mice undergoing the Omicron BA.1-RAMIHM procedure. With the analysis of heavy-chain (IGH) and light-chain (IGK) parings, we also mapped out the overall (Figure S3), enriched, and top 10 heavy- and light-chain V/J segment recombination patterns in these B cell populations (Figure 1F, Dataset S1). In summary, scBCR-seq data mapped the clonal repertoires and revealed enriched IgG clonotypes in the peripheral blood, plasma B cell, and memory B cell populations from the Omicron BA.1-RAMIHM humanized mouse.

## Identification of Omicron-specific functional mAb clones from top-ranked paired human Ig chains of Omicron BA.1-RAMIHM animals

To test whether the most enriched BCRs in these B cell populations are Omicron BA.1 reactive, we selected a panel of BCRs for recombinant mAb expression, including three top clones from peripheral blood, three top ones from plasma B cell populations, and 10 top clones from memory B cell populations (Figure 1G). To functionally analyze the antibody response to SARS-CoV-2 Omicron BA.1 RBD, we cloned paired heavy- and light-variable segments into human IgG1 expression vectors, and used the Expi293F mammalian expression system to produce selected mAbs. Thereafter, we used SARS-CoV-2 Omicron BA.1 RBD-specific ELISA to determine antibody binding by using transfected culture supernatants that contain secreted antibodies (Figure 2A). As a result, almost all (14/15 reactive) of the top enriched antibody clones collected from peripheral blood, plasma B cell, and memory B cell populations are recognized by recombinant Omicron BA.1 RBD proteins. Out of those positive mAbs, 10 of the selected clones showed potent binding affinity (Figure 1H, Dataset S2). These findings indicated that RAMIHM is a highly effective approach for generating and isolating antigen-specific mAbs.

To further characterize highly potent functional mAbs, we recombinantly expressed these 15 mAb candidate clones in a mammalian system and tested their neutralization ability against the Omicron BA.1 subvariant. By screening the mAbs from culture supernatants by neutralizing assay using a spike-based SARS-CoV-2 Omicron pseudovirus system, we found three clones with obvious neutralization activity against Omicron BA.1 pseudovirus (Figures S4A and S4B). We chose these top 3 clones (named PC.03, MB.02, and MB.08) for further development and characterization.

## Characterization of fully human lead clones with strong binding to Omicron BA.1 RBD

We then purified the three leading antibody clones, PC.03, MB.02, and MB.08, by affinity chromatography using Protein A beads and examined purity by SDS-PAGE (Figure S1E). Thereafter, purified antibodies were tested for SARS-CoV-2 Omicron BA.1 RBD reactivity by ELISA and monitored real-time association and dissociation to recombinant SARS-CoV-2 Omicron BA.1 RBD proteins using the Octet system. The ELISA titration result of the lead mAb clones vs. recombinant SARS-CoV-2 Omicron BA.1 RBD proteins showed that these three mAb clones

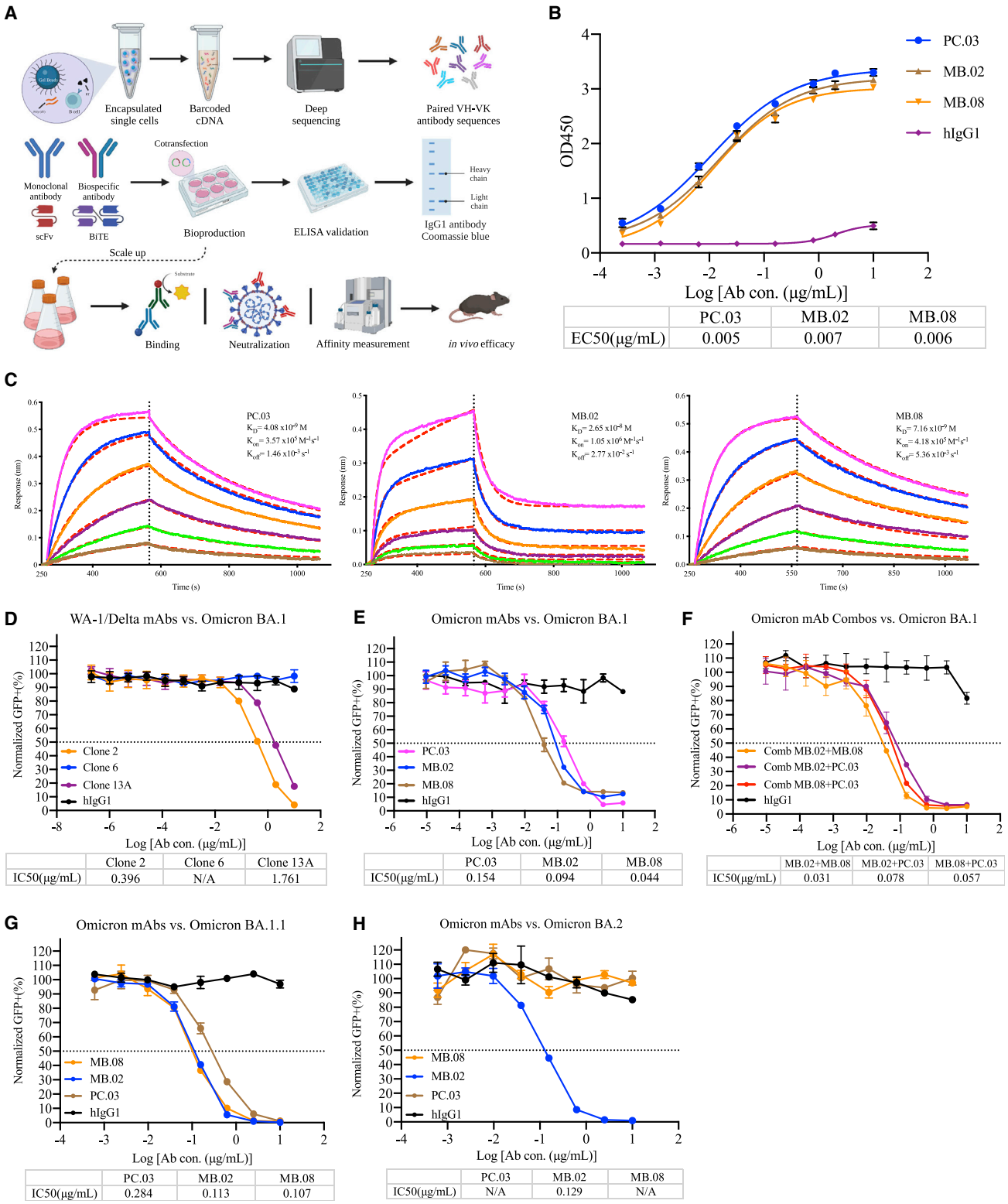


| | PC.03 | MB.02 | MB.08 |
|---|---|---|---|
| EC50(μg/mL) | 0.005 | 0.007 | 0.006 |

| | Clone 2 | Clone 6 | Clone 13A |
|---|---|---|---|
| IC50(μg/mL) | 0.396 | N/A | 1.761 |

| | PC.03 | MB.02 | MB.08 |
|---|---|---|---|
| IC50(μg/mL) | 0.154 | 0.094 | 0.044 |

| | MB.02+MB.08 | MB.02+PC.03 | MB.08+PC.03 |
|---|---|---|---|
| IC50(μg/mL) | 0.031 | 0.078 | 0.057 |

| | PC.03 | MB.02 | MB.08 |
|---|---|---|---|
| IC50(μg/mL) | 0.284 | 0.113 | 0.107 |

| | PC.03 | MB.02 | MB.08 |
|---|---|---|---|
| IC50(μg/mL) | N/A | 0.129 | N/A |

**Figure 2. Biophysical and functional characterization of lead clones of Omicron BA.1-specific antibodies**

(A) Schematic illustration of human IgG1 mAb reconstruction, production, and validation.

(B) Graph shows leading Omicron mAbs reactivity. The ELISA $EC_{50}$ values were calculated by Prism V8.0 software using a four-parameter logistic curve fitting approach. Error bars represent the mean ± SEM of triplicates with individual data points in plots.

*(legend continued on next page)*

have $EC_{50}$ values at the level of ~0.01 μg/mL, suggesting that these mAbs can indeed tightly bind to Omicron BA.1 RBD ($EC_{50}$ < 8 ng/mL for all three clones) (Figure 2B). Octet results with his-tag Omicron BA.1 RBD antigen immobilization displayed ultra-strong binding ($K_D$ at 0.8 nM for MB.02, and $K_D$ <1 p.m. for PC.03 and MB.08) (Figure S1F). The avidity effect due to multivalent binding may have contributed to the results. Therefore, we performed the reverse Octet assay with antibody immobilization to measure the single-mAb binding affinity, and we found the affinity between these clones to Omicron BA.1 is within the low nanomolar range (Figure 2C). These $K_D$ values showed that the binding strengths of the three lead mAbs are stronger than that of hACE2 with Omicron BA.1 RBD (31.4 ± 11.62 nM).[22] Noted that most of the approved or emergency use authorization (EUA) mAbs have much weaker binding with Omicron BA.1 RBD[23,24] (summarized in Table S2). To further determine whether these leading mAbs compete for similar epitopes, we performed epitope binning experiments by Octet using an in-tandem assay. The results have revealed that PC.03, MB.02, and MB.08 likely share overlapping epitopes (Figure S4C).

## Further characterization of fully human leading neutralization mAb clones against other circulating Omicron subvariants

We then performed neutralization assays for the three leading mAbs in purified form, along with other mAbs. We previously identified and developed several potent and specific mAbs against the ancestral virus and the Delta variant, namely clone 2, clone 6, and clone 13A.[25] In a pseudovirus neutralization assay, we found that while clone2 and clone13A can still neutralize the Omicron BA.1 subvariant, the potency is significantly reduced (by one to two orders of magnitude in terms of $IC_{50}$ values, at 0.396 and 1.761 μg/mL for clone2 and clone13A, respectively) (Figure 2D), a phenomenon similar to other mAbs developed against the ancestral spike.[19,20] In contrast, all three leading clones, PC.03, MB.02, and MB.08, potently neutralized the Omicron BA.1 subvariant, with $IC_{50}$ values at 0.154 μg/mL (PC.03), 0.094 μg/mL (MB.02), and 0.044 μg/mL (MB.08) (Figures 2E and S4D). The neutralization potency of the three leading Omicron BA.1-specific mAb clones is much stronger than those of our prior mAbs and those under prior regulatory approval or EUAs (Table S2). These three mAbs, however, showed no neutralization against the Delta variant (Figure S4E), further suggesting that they are Omicron BA.1 specific.

To test if these clones can be used in combination, we performed neutralization assays by combining two clones. Interestingly, despite epitope overlap, these mAb clones can still slightly improve each other's neutralization capacity, with the most effective combination being an antibody cocktail of MB.02 + MB.08 ($IC_{50}$ = 0.031 μg/mL) against pseudotyped SARS-CoV-2 Omicron variant (Figure 2F). Meanwhile, to test if these Omicron mAbs can be targeted on other Omicron sublineages (BA.1.1, BA.2, BA.2.12.1, BA.3, and BA.5), we conducted a pseudovirus neutralization assay. The findings suggested that all three leading clones can maintain potency to Omicron BA.1.1, with $IC_{50}$ values at 0.284 μg/mL (PC.03), 0.113 μg/mL (MB.02), and 0.107 μg/mL (MB.08) (Figure 2G). However, two (PC.03 and MB.08) of the top clones showed no neutralization to Omicron BA.2, and only MB.02 retains potency to Omicron BA.2, with $IC_{50}$ values at 0.129 μg/mL (PC.03) (Figure 2H). Moreover, MB.02 also maintains potency against current circulating Omicron subvariants, with $IC_{50}$ values at 0.433 μg/mL (BA.2.12.1), 0.131 μg/mL (BA.3), and 0.395 μg/mL (BA.5). In summary, these potent neutralizing mAbs showed that they have high affinity vs. Omicron BA.1 RBD and strong potency in pseudovirus neutralization, which are at least two orders of magnitude more potent than existing clinically approved or authorized SARS-CoV-2 mAbs. The findings revealed that the leading clone (MB.02) had the capacity to neutralize all tested pseudoviruses of Omicron sublineages.

## Application of RAMIHM on CD22

To better understand the breadth of the RAMIHM, we next focused on cancer surface antigens and selected CD22 as a target. CD22, a single-pass transmembrane protein (Figure 3A), is a well-known therapeutic target for the treatment of B cell malignancies and systemic autoimmune diseases.[26–28] To rapidly obtain fully human paired variable sequences of CD22-specific

(C) Binding characteristics of the neutralizing mAbs determined by using bio-layer interferometry (BLI). Purified mAbs were immobilized onto an Anti-Human Fc Capture (AHC) sensor, and all measurements were performed by using a serial 2-fold dilution of soluble SARS-CoV-2 Omicron BA.1 RBD, starting from 50 nM (magenta) to 1.56 nM (brown). Global fit curves are shown as red dashed lines. The vertical black dotted-dashed lines indicate the transition between the association and disassociation phases.

(D) Neutralization assay of SARS-CoV-2 Omicron BA.1 pseudovirus by WA-1/Delta mAbs. The graph shows the normalized relative GFP signals for detection of HEK293T cells expressing hACE2, 24 h after infection with SARS-CoV-2 Omicron BA.1 pseudovirus, in the presence of an increasing concentration of indicated WA-1/Delta mAbs.

(E) Neutralization assay of SARS-CoV-2 Omicron BA.1 pseudovirus by leading Omicron mAbs. The graph shows the normalized relative GFP signals for detection of HEK293T cells expressing hACE2, 24 h after infection with SARS-CoV-2 Omicron BA.1 pseudovirus, in the presence of an increasing concentration of indicated Omicron mAbs.

(F) Neutralization assay of SARS-CoV-2 Omicron BA.1 pseudovirus by leading Omicron mAb combinations. The graph shows the normalized relative GFP signals for detection of HEK293T cells expressing hACE2, 24 h after infection with SARS-CoV-2 Omicron BA.1 pseudovirus, in the presence of an increasing concentration of indicated Omicron mAb combinations (MB.02 + MB.08, MB.08 + PC.03, MB.02 + PC.03).

(G) Neutralization assay of SARS-CoV-2 Omicron BA.1.1 pseudovirus by leading Omicron mAbs. The graph shows the normalized relative GFP signals for detection of HEK293T cells expressing hACE2, 24 h after infection with SARS-CoV-2 Omicron BA.1.1 pseudovirus, in the presence of an increasing concentration of indicated Omicron mAbs.

(H) Neutralization assay of SARS-CoV-2 Omicron BA.2 pseudovirus by leading Omicron mAbs. The graph shows the normalized relative GFP signals for detection of HEK293T cells expressing hACE2, 24 h after infection with SARS-CoV-2 Omicron BA.2 pseudovirus, in the presence of an increasing concentration of indicated Omicron mAbs. The $IC_{50}$ values were calculated by Prism V8.0 software using a four-parameter logistic curve fitting approach. The dashed line indicates a 50% reduction in viral infectivity. Error bars represent the mean ± SEM of triplicates with individual data points in plots. Source data and additional statistics for experiments are in supplemental excel file(s). See also Figures S1–S4.

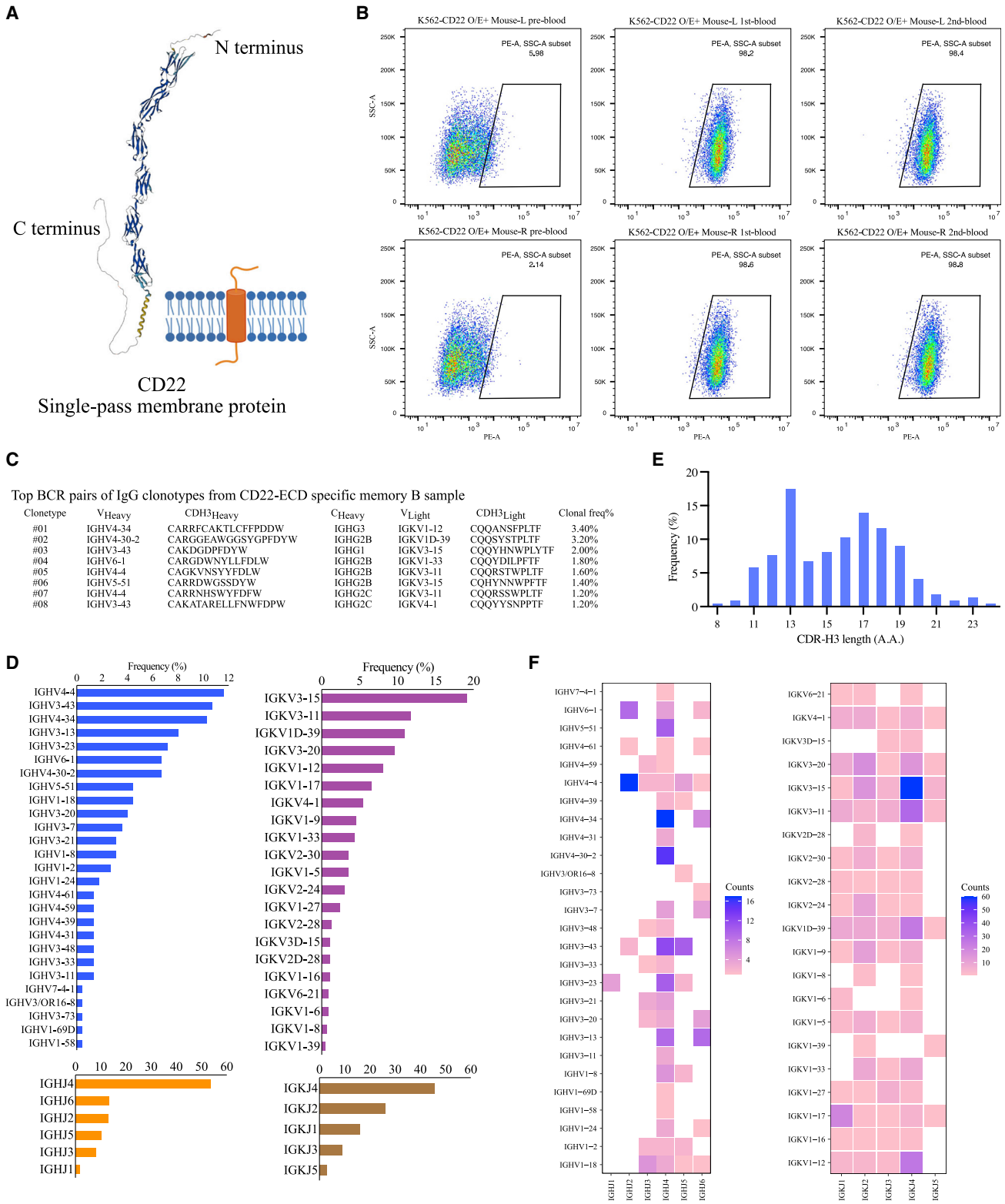


**Figure 3. Evaluation of CD22-RAMIHM humanized mice and rapidly identified fully human CD22-specific monoclonal antibodies**

(A) The structure of human CD22 protein predicted (UniProt: 060926) by AlphaFold Protein Structure Database

(B) CD22 antibody titer measurement in plasma samples. All plasma samples were diluted into 1:200, then incubated with K562-CD22 O/E cells and detected by flow cytometry. Data from two CD22-RAMIHM mice are shown.

*(legend continued on next page)*

antibodies, we firstly designed CD22-specific LNP-mRNAs. The open reading frame of CD22 was flanked by a 5′ untranslated region (UTR), 3′ UTR, and poly-A tail. Then, we encapsulated the transcribed CD22 mRNA into LNPs to generate CD22 LNP-mRNAs and proceeded to characterize the immunogenicity of CD22 LNP-mRNA *in vivo*. Four 10-μg doses and one 20-μg dose of CD22 specific mRNA-LNPs were administered to two IgG-humanized mice with retro-orbital blood samples collected from each humanized mouse before and after booster immunization. Blood samples were labeled as pre-, first, or second immunization draws depending on the collection sequence. Antibody titers were measured using a cell staining assay with 1:200 plasma dilution, and binding activity was determined using flow cytometry. Three sequential plasma samples showed increasing LNP-mRNA-elicited antibody responses during each blood collection (Figure 3B).

To acquire CD22-ECD binding B cells, we collected spleen and lymph nodes from a CD22-RAMIHM mouse, memory B cells were enriched by immunomagnetic negative selection, and 25 μg of recombinant CD22-ECD protein was used as bait to isolate CD22-ECD binding memory B cells from pre-enriched memory B cells. Subsequently, 10,000 positive memory B cells were counted and subjected to scBCR library preparation and sequencing. The clonotype enrichment was calculated based on the number of cells observed with identical pairs of heavy and light chains by analyzing the BCR repertoires. We mapped the landscape of BCR populations in CD22-RAMIHM mice Figure 3C). Meanwhile, the scBCR-seq data allowed us to further decipher potential germline genes associated with the response to CD22 LNP-mRNA immunization. We found that *IGHV4-4*, *IGHV3-43*, and *IGHV4-34* were the top three relative enriched IGHV genes, and *IGKV3-15* was the top enriched *IGKV* gene in CD22-RAMIHM mouse (Figure 3D, Dataset S1). In particular, we noticed that the *IGHJ4* germline gene is more frequently used than the other five *IGHJ* genes (Figure 3D, Dataset S1), and a range of HCDR3 lengths between 8 and 24 aa was observed (Figure 3E, Dataset S1). Furthermore, to provide a more detailed landscape of germline gene expression, we determined the *IGHV*/*IGHJ* and *IGKV*/*IGKJ* combination usage. The *IGHV*/*IGHJ* and *IGKV*/*IGKJ* combination usage showed that *IGHV4-4*/*IGHJ2, IGHV4-34*/*IGHJ4, IGHV4-30-2*/*IGHJ4*, and *IGKV3-15*/*IGKJ4* had greater expression in CD22-RAMIHM mouse (Figure 3F, Dataset S1). These data demonstrated that RAMIHM can be rapidly applied to cancer immunotherapy targets such as CD22 without the need for recombinant protein antigen expression.

## Application of RAMIHM on GPRC5D

GPRCD is an orphan G protein-coupled receptor, which has been identified as an intriguing clinical target for immunotherapy of multiple myeloma in B-cell maturation antigen (BCMA) antigen-escaped models.[29] It remains, however, technically challenging to obtain the natural conformation of GPRC5D proteins. Only a short N terminus and three small extracellular loops (ECLs) (Figure 4A) could be used as immunogens to generate peptide-specific antibodies. Furthermore, GPRC5D-overexpressing cells as immunogens combined with phage display screening have been reported to identify scFvs for CAR-T application,[30] which is limited by high-quality and well-validated phage display libraries. To demonstrate the applicability of RAMIHM in GPCR antibody development, we rapidly designed a GPRC5D-specific mRNA, where the open reading frame of GPRC5D flanked by a 5′ UTR, 3′ UTR, and poly-A tail. Then, we encapsulated the transcribed GPRC5D mRNA into LNPs to generate GPRC5D LNP-mRNA and proceeded to characterize the immunogenicity *in vivo*. Four 10-μg doses and one 20-μg dose of GPRC5D-specific mRNA-LNPs were administered to two IgG-humanized mice. Retro-orbital blood samples were collected from each humanized mouse before and after booster immunization. Blood samples were labeled as pre-, first, or second immunization draw depending on the collection sequence. Antibody titers were measured using a cell staining assay with 1:200 plasma dilution, and binding activity was determined using flow cytometry. Three sequential plasma samples showed increasing vaccine-elicited antibody responses during each blood collection (Figure 4B).

To acquire GPRC5D-specific B cells, we collected spleen and lymph nodes from a GPRC5D-RAMIHM mouse. Memory B cells were enriched by immunomagnetic negative selection and stained with mouse IgG1 and IgG2ab antibodies to isolate IgG isotype-positive memory B cells from pre-enriched memory B cells. Subsequently, 10,000 positive memory B cells were counted and subjected to scBCR library preparation and sequencing. The clonotype enrichment was calculated based on the number of cells observed with identical pairs of heavy and light chains. By analyzing the BCR repertoires, we mapped the landscape of BCR populations in the GPRC5D-RAMIHM mouse (Figure 4C, Dataset S1). Meanwhile, the scBCR-seq data allowed us to further decipher potential germline genes associated with the response to GPRC5D LNP-mRNAs immunization. Notably, one dominant IgG1 clone was observed. *IGHV3-43* and *IGKV1D-39* genes had highest frequencies in the GPRC5D-RAMIHM mouse (Figure 4D, Dataset S1). Furthermore, 24 of 31 *IGHV* genes were paired with *IGHJ6* (Figure 4F, Dataset S1), suggesting the *IGHJ6* gene was highly engaged by GPRC5D-RAMIHM immunization. Meanwhile, the *IGHJ6* gene is usually longer (has three to five more amino acids) than the other five *IGHJ* genes,[31] resulting in a long HCDR3 length in GPRC5D-RAMIHM mouse compared with the above CD22-RAMIHM mouse (Figure 4E, Dataset S1). These data demonstrated that RAMIHM can be rapidly applied to multi-transmembrane targets such as GPRC5D without the need for recombinant protein antigen expression.

To validate binding activity of those top enriched IgG1/IgG2ab+ clonotypes, we again cloned paired heavy- and light-variable segments into human IgG1 expression vectors and used the Expi293F mammalian expression system to produce individual clones of mAbs. We used cell staining assay to

(C) Single B cell variable chains for antibody cloning. Variable (V) genes and CDR3 lengths for paired heavy and light chains of top enriched clones to CD22 from single BCR sequencing.
(D) Distribution of heavy chain complementarity-determining region 3 (HCDR3) length in memory B cells from CD22-RAMIHM mouse.
(E) Global frequencies of IGHV, IGHJ, IGKV, and IGKJ genes usage in CD22-RAMIHM mouse.
(F) Numbers and diversifications of IGHV/IGHJ, IGKV/IGKJ gene combination usage in CD22-RAMIHM mouse. See also Figures S5 and S7.

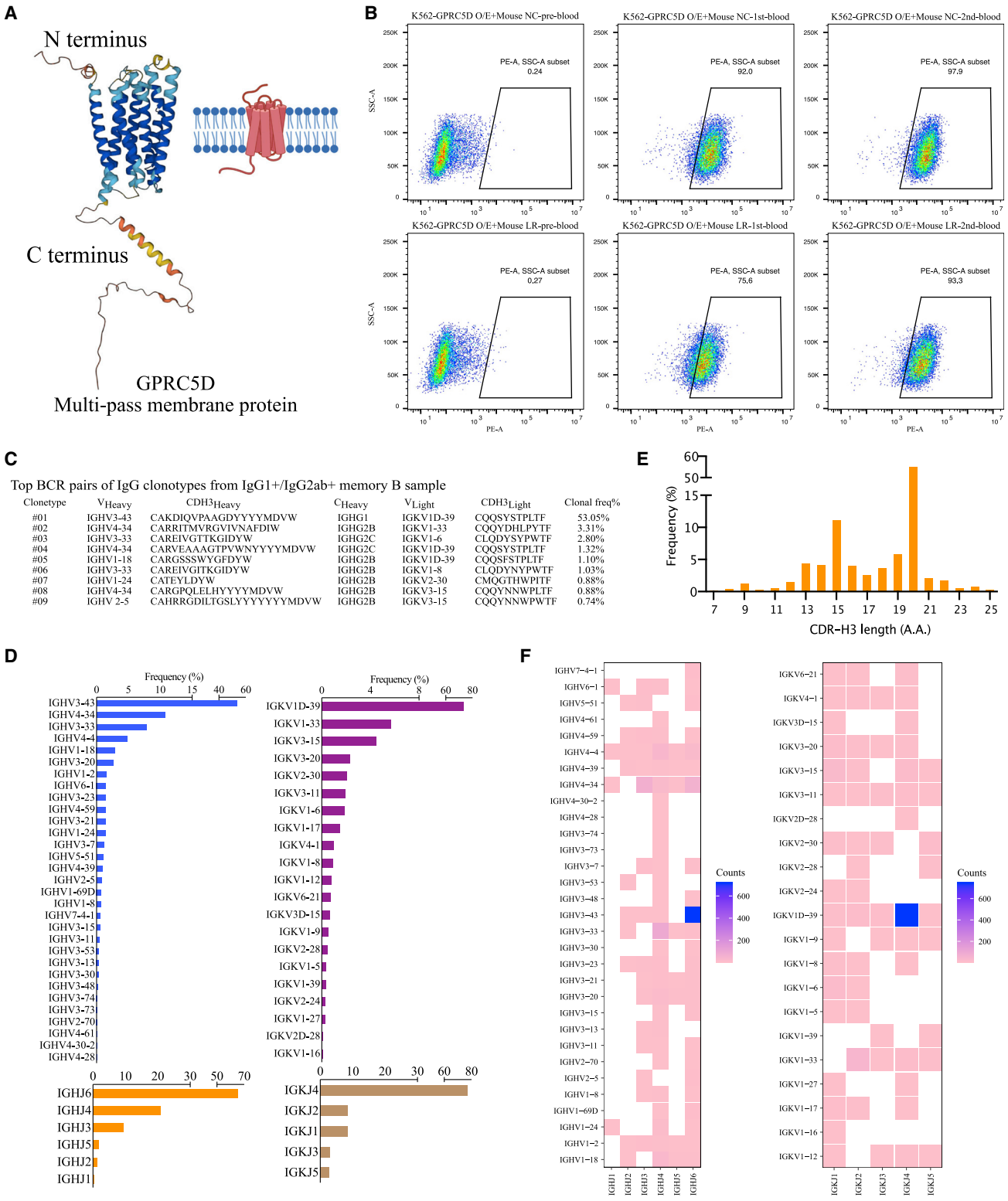


**Figure 4. Evaluation of GPRC5D-RAMIHM humanized mice and rapidly identified fully human GPRC5D-specific monoclonal antibodies**

(A) The structure of human GPRC5D protein predicted (UniProt: Q9NZD1) by AlphaFold Protein Structure Database.

(B) GPRC5D antibody titer measurement in plasma samples. All plasma samples were diluted into 1:200, then incubated with K562-GPRC5D O/E cells, and detected by flow cytometry. Data from two CD22-RAMIHM mice are shown.

*(legend continued on next page)*

determine antibody binding by using transfected culture supernatants that contain secreted antibodies. As a result, almost all of the top enriched IgG1/IgG2ab+ antibody clones (8/9, 90%) recognize GPRC5D-overexpressed K562 cells, with varying levels of cells staining positive (Figure S6), potentially due to different binding affinities. Out of these positive mAbs, two clones (clone 2 and clone 8) showed the most potent binding affinity (Figure S6). These data again validated that RAMIHM is a highly effective approach for rapid development of target-specific human mAbs against challenging targets.

### Evaluation of background BCR repertoire

To further evaluate technical features of RAMAHM, we characterized the baseline of B cell clonal levels in the non-RAMAHM-immunized humanized mouse. We collected spleen, bone marrow, and whole blood from a non-RAMAHM-immunized humanized mouse, followed by previously established processes to isolate desired B cell subsets (memory B, plasma B, PBMC) for comparison. Then, 10,000 fresh cells from each B cell subset were subjected to scBCR library construction and sequencing. However, the library construction reaction cannot amplify the IgGH and IgK repertoires from the cDNA of the non-immunized humanized mouse's PBMC library, indicating that there were rare or undetectable $IgG^+$ B cells in the blood if the mouse is not immunized. Meanwhile, the different density of PCR bands was amplified from different B cell libraries, indirectly reflecting the natural baseline levels of $IgG^+$ B cells in different organs in a non-immunized mouse (Figure S7A, Dataset S1). Furthermore, though scBCR-seq data, we analyzed and compared the natural frequencies of *IGHV, IGHJ, IGKV*, and *IGKJ* gene usage between the memory B library and plasma B library. The results revealed that there is no strong correlation between the two B cell libraries, and no significant pre-enriched B cell clonotypes were observed in non-immunized humanized mouse (Figures S7C and S7D). *IGHJ4* and *IGKJ4* genes were preferentially engaged in non-immunized humanized mouse, which led to a similar distribution and scope of HCDR3 length between the two samples (Figure S7B). Subsequently, to further investigate the patterns of antibody isotype distribution between non-RAMAHM mouse and Omicron BA.1 RAMAHM mouse, we compared the two sets of scBCR-seq data and found IgG2B was abundantly expressed in response to Omicron BA.1 RAMAHM, where nearly ~40% of IgG2B clonotypes were elevated in Omicron BA.1-enriched memory B library, and ~20% were elevated in CD138-enriched plasma B library, indicating the naive B cells underwent isotype switching during Omicron BA.1 RAMAHM induction (Figure S7E). Additionally, the *IGHV/IGHJ* combination usage in the Omicron BA.1 RAMAHM mouse showed significantly different patterns from those of non-immunized humanized mouse (Figure S7F). A total of 63 distinct *IGHV/IGHJ* combinations were discovered in the Omicron BA.1-enriched memory B library, and 22 distinct ones were observed in the CD138-enriched plasma B library, reflecting increased clonal expansion and diversification of B cells against Omicron BA.1 during RAMAHM induction (Figure S7F).

## DISCUSSION

GPCRs are multispan transmembrane proteins with important biological and pathological roles. Therefore, it is hard to isolate the full length of GPCRs with native conformations using current protein purification methods. In addition, the N terminus and small ECLs of GPCRs are the most common materials that are used as immunogens for regular anti-GPCR antibody generation. However, employing those disordered truncated peptides in current antibody discovery platforms (such as mouse immunization and *in vitro* display techniques) often leads to generating peptide-specific antibodies that are unable to recognize the native form of the target proteins. The mRNA-based vaccines against SARS-CoV-2 can successfully elicit broad and potent antibody responses when administered intramuscularly, indicating that LNP-encapsulated mRNA can be used to achieve protein expression and thereby antigen-specific immunization *in vivo*. This method could overcome a major obstacle in developing mAbs against challenging targets like multi-transmembrane proteins.

To provide a simple and better platform for antibody discovery, we developed a highly effective animal immunization approach (RAMIHM) combined with high-throughput customized scBCR-seq. In contrast with the current established antibody discovery platform, RAMIHM enables us to isolate antigen-specific antibodies within 2 weeks, offering the opportunity to rapidly respond to the potential risks of emerging infectious viruses or variants. Meanwhile, RAMIHM does not need human samples and is fully controllable in the laboratory. Most importantly, RAMIHM is faster than conventional protein-based immunization methods and highly maintains the target protein in a natural conformation, thereby enhancing immunogenicity and antigenicity and generating antibodies with *in vivo* affinity maturation process (Table S1). Overall, the mAbs developed by RAMIHM are fully human and compatible with downstream drug development and/or translational studies.

To quickly provide countermeasures to upcoming VoCs such as the Omicron variant. We rapidly identified 15 anti-Omicron BA.1 mAbs from Ig humanized mice by RAMIHM within 2 weeks. Among those mAbs, three of them were further validated as potent neutralizing mAbs. MB.08 showed the highest binding capacity ($K_D$ = 7 nM) and strongest neutralizing ability against pseudotyped viruses of SARS-CoV-2 Omicron BA.1 ($IC_{50}$ = 44 ng/mL), and MB.02 exhibited a broad-spectrum neutralizing capacity to adequately cover all major sublineages of the Omicron variant (BA.1, BA.1.1, BA.2, BA.2.12.1, BA.3, BA.5). Meanwhile, an antibody cocktail combining MB.08 with MB.02 exhibited enhanced SARS-CoV-2 Omicron neutralization potency ($IC_{50}$ = 30 ng/mL) compared with individual clones, although the epitope binning experiment results suggested that

(C) Single B cell variable chains for antibody cloning. Variable (V) genes and CDR3 lengths for paired heavy and light chains of top enriched clones to GPRC5D from single BCR sequencing.
(D) Distribution of heavy chain complementarity-determining region 3 (HCDR3) length in memory B cells from GPRC5D-RAMIHM mouse.
(E) Global frequencies of IGHV, IGHJ, IGKV, and IGKJ genes usage in GPRC5D-RAMIHM mouse.
(F) Numbers and diversifications of IGHV/IGHJ, IGKV/IGKJ gene combination usage in GPRC5D-RAMIHM mouse. See also Figures S5–S7.

MB.08 might bind to sites in Omicron spike RBD that are similar to those found in PC.03 and MB.02. Furthermore, we continued to utilize RAMIHM on cancer immunotherapy targets. We observed that antigen-specific IgG-positive antibody titers continued to increase during the first week after RAMIHM onset and remained at a peak level until the endpoint. Combined with high-throughput scBCR-seq, we were able to examine B cell clonotype enrichment and efficiently identify the paired antibodies sequences from RAMIHM-treated humanized mice. Another significant advantage of RAMIHM is that fully human mAb candidates against a specific target can be developed from as few as one single humanized mouse. In brief, summary, RAMIHM can serve as a versatile platform broadly applicable to antibody discovery against emerging pathogens or other therapeutic targets.

### Limitations of the study

RAMIHM uses mRNA to encode antigen. This study used mRNAs encoding full-length transmembrane proteins, which can induce immune responses to all possible regions of the protein, including intracellular domains. Thus, the antibodies reacting to those domains might not be desired. Specific domains can be encoded in future studies. RAMIHM requires IgG-humanized mice, which currently has limited availability. Finally, scBCR-seq occasionally detects unpaired BCR clones, with only IgH or IgK/IgL sequence(s).

### Significance

Development of fully human, potent, and specific monoclonal antibodies (mAbs) has profound research and clinical implications. Existing antibody development methods have their own limitations. Here, we developed RAMIHM, a highly efficient strategy that allows us to generate fully human mAbs within several weeks using LNP-mRNA immunization followed by scBCR-seq. This approach allows us to, first, bypass the protein antigen purification step for difficult multi-transmembrane proteins and, secondly, immunize humanized animals with natural conformation of antigen expressed from the hosts' cells *in vivo*. Our study demonstrated that RAMIHM can be a versatile platform for antibody discovery against emerging pathogens and other therapeutic targets.

## STAR★METHODS

Detailed methods are provided in the online version of this paper and include the following:

- KEY RESOURCES TABLE
- RESOURCE AVAILABILITY
  - Lead contact
  - Materials availability
  - Data and code availability
- EXPERIMENTAL MODEL AND SUBJECT DETAILS
  - Health/immune status
  - Whether subjects were involved in previous procedures
  - Whether the subject is drug or test naive
  - Housing and husbandry conditions of experimental animals
- METHOD DETAILS
  - Rapid mRNA immunization of humanized mice
  - ELISA analysis for plasma and mAb supernatant binding to omicron RBD protein
  - Humanized mice B cell isolation and purification
  - Single-cell VDJ sequencing and data analysis
  - *In vitro* generation of recombinant mAbs
  - Omicron pseudovirus generation and neutralization assay
  - Antibody binding kinetics, epitope mapping by biolayer interferometry (BLI)
  - Antibody clone cellular binding testing
  - Chemical compounds
  - Oligo sequences
- QUANTIFICATION AND STATISTICAL ANALYSIS
  - Standard statistics
  - Schematic illustrations
  - Replication, randomization, blinding and reagent validations
- ADDITIONAL RESOURCES

### SUPPLEMENTAL INFORMATION

Supplemental information can be found online at https://doi.org/10.1016/j.chembiol.2022.12.005.

### ACKNOWLEDGMENTS

We thank various members from our labs for discussions and support. We thank staff from various Yale core facilities (Keck, YCGA, HPC, YARC, CBDS, and others) for technical support. We thank Drs. Tsemperouli, Karatekin, Lin, and others for providing equipment and related support. We thank various support from the Department of Genetics; Institutes of Systems Biology and Cancer Biology; Dean's Office of Yale School of Medicine; and the Office of Vice Provost for Research.

S.C. is supported by NIH/NCI/NIDA (DP2CA238295, R01CA231112), DoD (W81XWH-21-1-0019, W81XWH-20-1-0072, W81XWH-21-1-0514), Alliance for Cancer Gene Therapy, and Pershing Square Sohn Cancer Research Alliance.

### AUTHOR CONTRIBUTIONS

S.C. conceived RAMIHM and designed with P.R. and L.P. P.R. led and performed the majority of experiments and data analysis in all figures except NGS. L.P. performed LNP-mRNA optimization, animal immunization, sample collection, and mAb clone characterization. L.Y., K.S., Q.L., M.B., T.L., and P.C. assisted with the experiments. Z.F. packaged and characterized the Omicron BA1 LNP-mRNA. D.K. provided support on Octet. K.S. and P.A.R. analyzed NGS data. P.R. drafted the manuscript and figures with inputs from all authors, edited by L.P., K.S., P.A.R., and S.C. S.C. secured funding and supervised the work.

### DECLARATION OF INTERESTS

Yale filed a patent application on the technology. S.C. is a (co)founder of Cellinfinity Bio, EvolveImmune Tx, Chen Consulting (SCC) and Chen Tech (SCTH), all unrelated to the study.

Received: March 4, 2022
Revised: October 17, 2022
Accepted: December 19, 2022
Published: January 12, 2023

### REFERENCES

1. Mullard, A. (2021). FDA approves 100th monoclonal antibody product. Nat. Rev. Drug Discov. *20*, 491–495. https://doi.org/10.1038/d41573-021-00079-7.

2. Yang, D., Zhou, Q., Labroska, V., Qin, S., Darbalaei, S., Wu, Y., Yuliantie, E., Xie, L., Tao, H., Cheng, J., et al. (2021). G protein-coupled receptors: structure- and function-based drug discovery. Sig. Transduct. Target. Ther. *6*, 7. https://doi.org/10.1038/s41392-020-00435-w.

3. Zhang, X., Dong, S., and Xu, F. (2018). Structural and druggability landscape of frizzled G protein-coupled receptors. Trends Biochem. Sci. *43*, 1033–1046. https://doi.org/10.1016/j.tibs.2018.09.002.

4. Ruat, M., Hoch, L., Faure, H., and Rognan, D. (2014). Targeting of Smoothened for therapeutic gain. Trends Pharmacol. Sci. *35*, 237–246. https://doi.org/10.1016/j.tips.2014.03.002.

5. Wu, B., Chien, E.Y.T., Mol, C.D., Fenalti, G., Liu, W., Katritch, V., Abagyan, R., Brooun, A., Wells, P., Bi, F.C., et al. (2010). Structures of the CXCR4 chemokine GPCR with small-molecule and cyclic peptide antagonists. Science *330*, 1066–1071. https://doi.org/10.1126/science.1194396.

6. Mullard, A. (2018). FDA approves second GPCR-targeted antibody. Nat. Rev. Drug Discov. *17*, 613. https://doi.org/10.1038/nrd.2018.153.

7. Dolgin, E. (2018). First GPCR-directed antibody passes approval milestone. Nat. Rev. Drug Discov. *17*, 457–459. https://doi.org/10.1038/nrd.2018.103.

8. Cao, Y., Wang, J., Jian, F., Xiao, T., Song, W., Yisimayi, A., Huang, W., Li, Q., Wang, P., An, R., et al. (2022). Omicron escapes the majority of existing SARS-CoV-2 neutralizing antibodies. Nature *602*, 657–663. https://doi.org/10.1038/s41586-021-04385-3.

9. Hoffmann, M., Krüger, N., Schulz, S., Cossmann, A., Rocha, C., Kempf, A., Nehlmeier, I., Graichen, L., Moldenhauer, A.S., Winkler, M.S., et al. (2022). The Omicron variant is highly resistant against antibody-mediated neutralization: implications for control of the COVID-19 pandemic. Cell *185*, 447–456.e411. https://doi.org/10.1016/j.cell.2021.12.032.

10. Cele, S., Jackson, L., Khan, K., Khoury, D.S., Moyo-Gwete, T., Tegally, H., Scheepers, C., Amoako, D., Karim, F., Bernstein, M., et al. (2021). SARS-CoV-2 omicron has extensive but incomplete escape of pfizer BNT162b2 elicited neutralization and requires ACE2 for infection. Preprint at medRxiv. https://doi.org/10.1101/2021.12.08.21267417.

11. Fang, Z., Peng, L., Filler, R., Suzuki, K., McNamara, A., Lin, Q., Renauer, P.A., Yang, L., Menasche, B., Sanchez, A., et al. (2022). Omicron-specific mRNA vaccination alone and as a heterologous booster against SARS-CoV-2. Nat. Commun. *13*, 3250. https://doi.org/10.1038/s41467-022-30878-4.

12. Hutchings, C.J., Koglin, M., and Marshall, F.H. (2010). Therapeutic antibodies directed at G protein-coupled receptors. mAbs *2*, 594–606. https://doi.org/10.4161/mabs.2.6.13420.

13. Lopez Bernal, J., Andrews, N., Gower, C., Gallagher, E., Simmons, R., Thelwall, S., Stowe, J., Tessier, E., Groves, N., Dabrera, G., et al. (2021). Effectiveness of covid-19 vaccines against the B.1.617.2 (delta) variant. N. Engl. J. Med. *385*, 585–594. https://doi.org/10.1056/NEJMoa2108891.

14. Naranbhai, V., Garcia-Beltran, W.F., Chang, C.C., Berrios Mairena, C., Thierauf, J.C., Kirkpatrick, G., Onozato, M.L., Cheng, J., St Denis, K.J., Lam, E.C., et al. (2022). Comparative immunogenicity and effectiveness of mRNA-1273, BNT162b2 and Ad26.COV2.S COVID-19 vaccines. J. Infect. Dis. *225*, 1141–1150. https://doi.org/10.1093/infdis/jiab593.

15. Dejnirattisai, W., Shaw, R.H., Supasa, P., Liu, C., Stuart, A.S., Pollard, A.J., Liu, X., Lambe, T., Crook, D., Stuart, D.I., et al. (2022). Reduced neutralisation of SARS-CoV-2 omicron B.1.1.529 variant by post-immunisation serum. Lancet *399*, 234–236. https://doi.org/10.1016/S0140-6736(21)02844-0.

16. Hu, J., Peng, P., Cao, X., Wu, K., Chen, J., Wang, K., Tang, N., and Huang, A.L. (2022). Increased immune escape of the new SARS-CoV-2 variant of concern Omicron. Cell. Mol. Immunol. *19*, 293–295. https://doi.org/10.1038/s41423-021-00836-z.

17. Carreño, J.M., Alshammary, H., Tcheou, J., Singh, G., Raskin, A.J., Kawabata, H., Sominsky, L.A., Clark, J.J., Adelsberg, D.C., Bielak, D.A., et al. (2022). Activity of convalescent and vaccine serum against SARS-CoV-2 Omicron. Nature *602*, 682–688. https://doi.org/10.1038/s41586-022-04399-5.

18. Cele, S., Jackson, L., Khoury, D.S., Khan, K., Moyo-Gwete, T., Tegally, H., San, J.E., Cromer, D., Scheepers, C., Amoako, D.G., et al. (2022). Omicron extensively but incompletely escapes Pfizer BNT162b2 neutralization. Nature *602*, 654–656. https://doi.org/10.1038/s41586-021-04387-1.

19. Dejnirattisai, W., Huo, J., Zhou, D., Zahradník, J., Supasa, P., Liu, C., Duyvesteyn, H.M.E., Ginn, H.M., Mentzer, A.J., Tuekprakhon, A., et al. (2022). SARS-CoV-2 Omicron-B.1.1.529 leads to widespread escape from neutralizing antibody responses. Cell *185*, 467–484.e15. https://doi.org/10.1016/j.cell.2021.12.046.

20. Liu, L., Iketani, S., Guo, Y., Chan, J.F.W., Wang, M., Liu, L., Luo, Y., Chu, H., Huang, Y., Nair, M.S., et al. (2022). Striking antibody evasion manifested by the omicron variant of SARS-CoV-2. Nature *602*, 676–681. https://doi.org/10.1038/s41586-021-04388-0.

21. Planas, D., Saunders, N., Maes, P., Guivel-Benhassine, F., Planchais, C., Buchrieser, J., Bolland, W.H., Porrot, F., Staropoli, I., Lemoine, F., et al. (2022). Considerable escape of SARS-CoV-2 Omicron to antibody neutralization. Nature *602*, 671–675. https://doi.org/10.1038/s41586-021-04389-z.

22. Han, P., Li, L., Liu, S., Wang, Q., Zhang, D., Xu, Z., Han, P., Li, X., Peng, Q., Su, C., et al. (2022). Receptor binding and complex structures of human ACE2 to spike RBD from omicron and delta SARS-CoV-2. Cell *185*, 630–640.e10. https://doi.org/10.1016/j.cell.2022.01.001.

23. Cameroni, E., Bowen, J.E., Rosen, L.E., Saliba, C., Zepeda, S.K., Culap, K., Pinto, D., VanBlargan, L.A., De Marco, A., di Iulio, J., et al. (2022). Broadly neutralizing antibodies overcome SARS-CoV-2 Omicron antigenic shift. Nature *602*, 664–670. https://doi.org/10.1038/s41586-021-04386-2.

24. McCallum, M., Czudnochowski, N., Rosen, L.E., Zepeda, S.K., Bowen, J.E., Walls, A.C., Hauser, K., Joshi, A., Stewart, C., Dillen, J.R., et al. (2022). Structural basis of SARS-CoV-2 Omicron immune evasion and receptor engagement. Science *375*, 864–868. eabn8652. https://doi.org/10.1126/science.abn8652.

25. Peng, L., Hu, Y., Mankowski, M.C., Ren, P., Chen, R.E., Wei, J., Zhao, M., Li, T., Tripler, T., Ye, L., et al. (2022). Monospecific and bispecific monoclonal SARS-CoV-2 neutralizing antibodies that maintain potency against B.1.617. Nat. Commun. *13*, 1638. https://doi.org/10.1038/s41467-022-29288-3.

26. Tan, Y., Cai, H., Li, C., Deng, B., Song, W., Ling, Z., Hu, G., Yang, Y., Niu, P., Meng, G., et al. (2021). A novel full-human CD22-CAR T cell therapy with potent activity against CD22(low) B-ALL. Blood Cancer J. *11*, 71. https://doi.org/10.1038/s41408-021-00465-9.

27. Dörner, T., Shock, A., and Smith, K.G.C. (2012). CD22 and autoimmune disease. Int. Rev. Immunol. *31*, 363–378. https://doi.org/10.3109/08830185.2012.709890.

28. Xiao, X., Ho, M., Zhu, Z., Pastan, I., and Dimitrov, D.S. (2009). Identification and characterization of fully human anti-CD22 monoclonal antibodies. mAbs *1*, 297–303. https://doi.org/10.4161/mabs.1.3.8113.

29. Mailankody, S., Devlin, S.M., Landa, J., Nath, K., Diamonte, C., Carstens, E.J., Russo, D., Auclair, R., Fitzgerald, L., Cadzin, B., et al. (2022). GPRC5D-Targeted CAR T cells for myeloma. N. Engl. J. Med. *387*, 1196–1206. https://doi.org/10.1056/NEJMoa2209900.

30. Smith, E.L., Harrington, K., Staehr, M., Masakayan, R., Jones, J., Long, T.J., Ng, K.Y., Ghoddusi, M., Purdon, T.J., Wang, X., et al. (2019). GPRC5D is a target for the immunotherapy of multiple myeloma with rationally designed CAR T cells. Sci. Transl. Med. *11*, eaau7746. https://doi.org/10.1126/scitranslmed.aau7746.

31. Zhang, Y., Yan, Q., Luo, K., He, P., Hou, R., Zhao, X., Wang, Q., Yi, H., Liang, H., Deng, Y., et al. (2022). Analysis of B Cell receptor repertoires reveals key signatures of the systemic B cell response after SARS-CoV-2 infection. J. Virol. *96*, e0160021. https://doi.org/10.1128/JVI.01600-21.

## STAR★METHODS

### KEY RESOURCES TABLE

| REAGENT or RESOURCE | SOURCE | IDENTIFIER |
|---|---|---|
| Antibody | | |
| Goat anti-human IgG(H + L)/HRP | Fisher Scientific | Cat # 31412 |
| Goat anti-mouse IgG(H + L)/HRP | Fisher Scientific | Cat # A-10677 |
| PE–anti-human FC antibody | Biolegend | Cat#409304 |
| Anti-SARS-CoV-2 mAb (Clone 2) | Sidi Chen Lab | Peng et al. 2022[25] |
| Anti-SARS-CoV-2 mAb (Clone 6) | Sidi Chen Lab | Peng et al. 2022[25] |
| Anti-SARS-CoV-2 mAb (Clone 13A) | Sidi Chen Lab | Peng et al. 2022[25] |
| Anti-Omicron mAb (MB.02) | Sidi Chen Lab | This study |
| Anti-Omicron mAb (MB.08) | Sidi Chen Lab | This study |
| Anti-Omicron mAb (PB.03) | Sidi Chen Lab | This study |
| Bacterial and virus strains | | |
| B.1.1.529 variant (Omicron) pseudovirus | Sidi Chen Lab | This study |
| B.1.617 variant (Delta) pseudovirus | Sidi Chen Lab | This study |
| Omicron subvariant BA.1.1 pseudovirus | Sidi Chen Lab | This study |
| Omicron subvariant BA.2 pseudovirus | Sidi Chen Lab | Fang et al. 2022 [11] |
| Omicron subvariant BA.2.12.1pseudovirus | Sidi Chen Lab | This study |
| Omicron subvariant BA.3 pseudovirus | Sidi Chen Lab | This study |
| Omicron subvariant BA.5 pseudovirus | Sidi Chen Lab | This study |
| Chemicals, peptides, and recombinant proteins | | |
| DPBS | Kline | Cat#14190144 |
| RPMI 1640 Medium | Gibco | Cat#11875-093 |
| Fetal Bovine Serum | Sigma Aldrich | Cat#F4135-500ML |
| DMEM | Kline | Cat#11995065 |
| Penicillin-Streptomycin (10,000 U/mL) | Gibco | Cat#15140122 |
| Glutamax | Med School | Cat#35050061 |
| TWEEN 20 | Sigma-Aldrich | Cat# P1379 |
| 50TS microplate washer | Fisher Scientific | Cat#BT50TS16 |
| ACK Lysing Buffer | Lonza | Cat#BP10-548E |
| Gibson Assembly Master Mix - 50 rxn | NEB | Cat#E2611L |
| HiscribeTM T7 ARCA mRNA Kit (with tailing) | NEB | Cat#E2060S |
| Phusion Flash High-Fidelity PCR Master Mix | ThermoFisher | Cat#F548L |
| E-Gel™ Low Range Quantitative DNA Ladder | ThermoFisher | Cat#12373031 |
| QIAquick Gel Extraction Kit | Qiagen | Cat#28706 |
| EndoFree® Plasmid Maxi Kit | Qiagen | Cat#12362 |
| Quant-iT™ RiboGreen™ RNA Assay Kit | ThermoFisher | Cat#R11490 |
| Tetramethylbenzidine substrate | Biolegend | Cat#421101 |
| RNeasy® Plus Mini Kit | Qiagen | Cat#74134 |
| Library Construction Kit, 16 rxns | 10X Genomics | Cat#1000190 |
| Live/Dead aqua fixable stain | Thermofisher | Cat#L34976 |
| BSA | Fisher Scientific | BP1600-100 |
| 100 μm cell strainer | Corning | Cat#352360 |
| 40 μm cell strainer | Corning | Cat#352340 |
| BSA | Sigma Aldrich | Cat#A9418-100G |
| EDTA | Kline | Cat#AB00502-01000 |
| Tris-Cl pH 8.5 | TENOVA | Cat#15085 |

(*Continued on next page*)

*Continued*

| REAGENT or RESOURCE | SOURCE | IDENTIFIER |
|---|---|---|
| N1-Methylpseudouridine-5′-Triphosphate - (N-1081) | TriLink (NC) | Cat#N-1081-1 |
| Sucrose | Thomas | Cat#C987K85 (EA/1) |
| Lymphoprep | STEMCELL | Cat # 07851 |
| Memory B Cell Isolation Kit, mouse | Miltenyi Biotec | Cat#130-095-838 |
| CD138+ Plasma Cell Isolation Kit, mouse | Miltenyi Biotec | Cat#130-095-530 |
| rProtein A Sepharose Fast Flow | GE healthcare | Cat#17-1279-01 |
| Octet Anti-Penta-HIS (HIS1K) Biosensors | SARTORIUS | Cat#18-5120 |
| Octet Anti-Human Fc Capture (AHC) Biosensors | SARTORIUS | Cat#18-5060 |
| SARS-COV RBD protein (His-tag) | Fisher Scientific | Cat#50-196-4017 |
| SARS-COV2 Delta RBD protein (His-tag) | SINO | Cat#40592-V08H90 |
| SARS-COV2 Omicron RBD protein (His-tag) | SINO | Cat#40592-V08H121 |
| MERS-COV RBD protein (His-tag) | Fisher Scientific | Cat#50-201-9463 |
| ACE2 protein, Human, Recombinant (His Tag) | SINO | Cat # 10108-H08H |
| ACE2 protein, Human, Recombinant (mFc Tag) | SINO | Cat # 10108-H05H |
| Chromium Next GEM Single Cell 5′ Kit v2, 16 rxns PN-1000263 | 10X Genomics | Cat#PN-1000263 |
| Chromium Next GEM Chip K Single Cell Kit, 1 6 rxns PN-1000287 | 10X Genomics | Cat#PN-1000287 |
| CD22-ECD protein (His-tag) | SINO | Cat#11958-HNAH |
| **Experimental models: cell lines** | | |
| HEK293T | ThermoFisher | Catalog Number: R70007 |
| K562-CD22-O/E-GFP | Sidi Chen Lab | This study |
| K562-GPRC5D-O/E-GFP | Sidi Chen Lab | This study |
| **Experimental models: Organisms/strains** | | |
| ATX-GK + Human Transgenic Mouse | Alloy | N/A |
| **Oligo name and sequence** | | |
| Various oligos (See Table S3 - supplemental oligos file) | Sidi Chen Lab | This study |
| **Recombinant DNA** | | |
| pcDNA3.1 plasmids | Addgene | Cat# V790-20 |
| pHIVNLGagPol | Schmidt et al., 2020 | Gift from Dr Bieniasz' lab |
| pCCNanoLuc2AEGFP | Schmidt et al., 2020 | Gift from Dr Bieniasz' lab |
| pSARS-CoV-2 SΔ19 | Schmidt et al., 2022 | Gift from Dr Bieniasz' lab |
| pFZ47 (B.1.1.529 variant (6P)) | Sidi Chen Lab | Fang et al. 2022[11] |
| pVP29b (B.1.617 variant (6P)) | Sidi Chen Lab | Peng et al. 2022[25] |
| pCCNanoLuc2AEGFP plasmid | Schmidt et al. | Gift from Dr Bieniasz' lab |
| Polyethylenimine | POLYSCIENCES INC | Cat#24765-1 |
| pFZ57 (Omicron BA.2 subvariant (6P)) | Sidi Chen Lab | Fang et al. 2022[11] |
| pPR158 (Omicron BA.1.1 subvariant (6P)) | Sidi Chen Lab | This study |
| pPR185 (Omicron BA.2.12.1 subvariant (6P)) | Sidi Chen Lab | This study |
| pPR186 (Omicron BA.3 subvariant (6P)) | Sidi Chen Lab | This study |
| pPR187 (Omicron BA.5 subvariant (6P)) | Sidi Chen Lab | This study |
| pZF46 (B.1.1.529 Omicron spike hexapro mRNA) | Sidi Chen Lab | Fang et al. 2022[11] |
| pPR128 (CD22-mRNA) | Sidi Chen Lab | This study |
| pPR109 (GPRC5D-mRNA) | Sidi Chen Lab | This study |
| **Software and algorithms** | | |
| FlowJo software 9.9.6 | FlowJo, LLC | https://www.flowjo.com |
| GraphPad Prism 8.0 | GraphPad Software Inc | https://www.graphpad.com/scientific-software/prism/ |
| Pymol | Schrödinger | http://www.pymol.org/ |

(*Continued on next page*)

*Continued*

| REAGENT or RESOURCE | SOURCE | IDENTIFIER |
|---|---|---|
| Cell Ranger v3.1.0 | 10X Genomics | https://support.10xgenomics.com/single-cell-gene-expression/software/pipelines/latest/installation |
| Loupe V(D)J Browser | 10X Genomics | https://support.10xgenomics.com/single-cell-vdj/software/visualization/latest/installation |
| R | R project | https://www.r-project.org |
| plyr R package | Wickham. (2011). Journal of S tatistical Software | http://www.jstatsoft.org/v40/i01/ |
| dplyr R package | Wickham et al., (2021). dplyr: A Grammar of Data Manipulation. R package version 1.0.7 | https://CRAN.R-project.org/package = dplyr |
| ggplot2 R package | Wickham. (2016). ggplot2: Elegant Graphics for Data Analysis. Springer-Verlag New York | https://ggplot2.tidyverse.org |
| stringr R package | Hadley Wickham (2019). stringr: Simple, Consistent Wrappers for Common String Operations. R package version 1.4.0 | https://CRAN.R-project.org/package = stringr |
| Circlize R package | Gu et al., Bioinformatics, 2014 | https://cran.r-project.org/package = circlize |
| Pheatmap R package | Kolde, 2019 | https://cran.r-project.org/package = pheatmap |
| Deposited data | | |
| Single cell BCR-seq | This study | GEO: GSE203030 |
| Flow data | This study | Mendeley Data, https://doi.org/10.17632/4dcgs8mvzx.3 |

## RESOURCE AVAILABILITY

### Lead contact

Requests for further information or reagents should be directed to the lead contact and corresponding author, Sidi Chen (sidi.chen@yale.edu).

### Materials availability

Materials described in this study will be made available, either via public repository, or upon reasonable request with a Material Transfer Agreement.

### Data and code availability

All data generated or analyzed during this study are included in this article and its supplementary information files. Specifically, source data and statistics for non-high-throughput experiments are provided in a supplementary table excel file. The ATX humanized mice are available via Alloy Therapeutics.

NGS data have been deposited at GEO and are publicly available as of the date of publication. Accession number (GSE203030) is listed in the key resources table.

Flow data have been deposited at Mendeley Data and are publicly available as of the date of publication. DOI (https://doi.org/10.17632/4dcgs8mvzx.1) is listed in the key resources table.

Code: This paper does not report original code. This study uses adapted version of existing computational pipelines. Computer codes related to this study is provided as a zip file in supplemental information.

Any additional information required to reanalyze the data reported in this work paper is available from the lead contact upon reasonable request.

## EXPERIMENTAL MODEL AND SUBJECT DETAILS

This study uses ATX-GK mice.

### Health/immune status
Mice (both sex) are healthy before immunization. LNP-mRNA immunization was performed for RAMIHM.

### Whether subjects were involved in previous procedures
No.

### Whether the subject is drug or test naive
Yes.

### Housing and husbandry conditions of experimental animals
Mice were housed in standard vivarium condition at YARC, with free access to water and food, ambient room temperature (approximately 22°C) and humidity-controlled. Mice were maintained on a 14h:10h light/dark cycle (07:00 to 21:00 light on). Mouse health checks were performed regularly. The general health of for all the mice in this study is in good condition (BAR: bright, alert and responsive) before the related experiments started. Mice, both female and male, aged 8–20 weeks were used for experiments.

## METHOD DETAILS

### Rapid mRNA immunization of humanized mice
The full-length Omicron spike sequence used in mRNA immunization was based on two North American patients identified on Nov23rd, 2021. The LNP-mRNA was generated as previously described.[11] Humanized mice with human IgG and IgK transgene knock-ins (ATX-GK, Alloy Therapeutics) were used for rapid mRNA immunization, according to an accelerated (two-week) vaccination schedule. Pre-immune plasma was collected from the mice before the initiation of immunization. The mice were primed with intramuscular injection of 10 μg Omicron LNP-mRNA and boosted on days 2, 4, and 7 with the same dose as prime. On day 11, three days before sacrifice, mice received a final boost with 20 μg Omicron LNP-mRNA. All mice were retro-orbital bled on days 7, and 14, and anti-plasma titers were evaluated using an immunoassay as described below.

### ELISA analysis for plasma and mAb supernatant binding to omicron RBD protein
Plasma was extracted from the surface layer by using SepMate-15 tubes with Lymphoprep gradient medium (StemCell Technologies) after centrifugation at 1200*g* for 20 min. Afterward, antibody titers in plasma against Omicron RBD were evaluated using a direct coating ELISA. 384-well microtiter plate (Corning) was coated with 3 μg/mL of Omicron RBD recombinant protein (Sino Biological 40,592-V08H121) in PBS at 4°Covernight. The plate was washed with standard wash buffer PBS-T (PBS containing 0.05% Tween 20) and blocked with blocking buffer (PBS containing 0.5% BSA) for 1 h at room temperature (RT). Either serially diluted plasma samples or mAbs supernatant were added to the plate and incubated for 1 h at RT. Wells were then washed and incubated with secondary goat anti-mouse IgG labeled with HRP (Fisher, Cat# A-10677) at 1:2500 dilution in a blocking buffer for 1h at RT. Thereafter, wells were developed using TMB substrate (Biolegend, 421,101) according to the manufacturer's protocol. The reactions were terminated with 1M $H_3PO_4$ after 20 min of incubation at RT and optical density (OD) was measured by a spectrophotometer at 450 nm (PerkinElmer EnVision 2105).

### Humanized mice B cell isolation and purification
Three sets of single B cells were collected: PBMC sample, Omicron RBD-specific memory B cell sample, and $CD138^+$ plasma B cell sample. PBMC cells were isolated from fresh whole blood by using SepMate-15 tubes with Lymphoprep gradient medium (StemCell Technologies) after centrifugation at 1200*g* for 20 min. Poured top layer solution that contained PBMCs from SepMate tubes to a new falcon tube and washed once with PBS+2%FBS, resuspended with PBS, and stored on ice until use.

According to the manufacturer's protocol, Omicron RBD-specific memory B cells were isolated from pre-enriched memory B cells by magnetic positive selection (Miltenyi Biotec, 130-095-838). Briefly, the spleen and lymph nodes were gently homogenized and red blood cells were lysed in ACK lysis buffer (Lonza). The remaining cells were washed with PBS with 2%FBS and filtered through with a 50mL falcon tube. Thereafter, memory B cells were labeled with a memory B cell biotin-antibody cocktail combined with anti-biotin microbeads and isolated using a magnetic rack. Enriched memory B cells were eluted and mixed with 25ug of Omicron RBD recombinant protein with his tag and incubated for 30mins on ice. After incubation, the complex was washed and then incubated with anti-his-APC antibodies and anti-APC microbeads. The final antigen-enrichment B cells were eluted in PBS and stored on ice until use.

Plasma B cells were collected by fragmenting and rinsing bone marrows with PBS containing 2% FBS. Non-plasma cells were labeled with a biotin-conjugated antibody cocktail combined with anti-biotin microbeads and separated using a magnetic rack according to the manufacturer's protocol (Miltenyi Biotec, 130-092-530). Purified plasma B cells were eluted and sequentially incubated with CD138 microbeads for an additional 15 min at 4°C. The final $CD138^+$ plasma B cells were eluted in PBS and stored on ice until use.

### Single-cell VDJ sequencing and data analysis
For each above collection, 10,000 cells were loaded on a Chromium Next GEM Chip K Single Cell Kit. Single-cell lysis and cDNA first-strand synthesis was performed using Chromium Next GEM Single Cell 5' Kit v2 according to the manufacturer's protocol. The

barcoded single-strand cDNA was isolated via a Dynabeads MyOne SILANE bead cleanup mixture. The cDNA was amplified by 14 PCR cycles and purified via SPRI bead cleanup (X0.6) according to the manufacturer's protocol. For BCR repertoire libraries, 2 μL of amplified cDNA underwent two rounds of Target Enrichment using nested custom primer pairs specific for BCR constant regions. The target enrichments for the heavy chain and light chain were performed in separate reactions. After each PCR reaction, the PCR products were subjected to double-sided size selection with SPRI bead cleanup (X0.6 followed by X0.8) The primers were designed by Alloy biotechnologies and synthesized by KECK.

25 ng of each target enrichment PCR product was combined, and used for library preparation, consisting of fragmentation, end repair, A-tailing, adaptor ligation (Library Construction Kit), and sample index PCR (Dual Index Kit TT Set A) according to the manufacturer's instructions. The final library was profiled and quantified using the D1000 ScreenTape assay (Agilent) for the TapeStation system. Libraries were sequenced by paired-end sequencing (26 × 91 bp) on an Illumina Miseq. All libraries were targeted for sequencing depth of 5,000 raw read pairs per cell.

For bioinformatics analysis, BCL data were converted to demultiplexed FASTQ files by the Illumina Miseq controller. These files were processed by using Cell Ranger v6.0.1 with default settings to align the reads to customized germline V and J gene references. The custom references were created by combining mouse constant genes along with human V(D)J genes. The consensus amino acid sequences of top-enriched clonotypes from each collection were selected by using the Loupe V(D)J Browser and cDNA sequences were synthesized for further molecular cloning and recombinant antibody expression.

### *In vitro* generation of recombinant mAbs

The cDNAs of paired heavy- and light-chains from top-enriched IgG clonotypes were codon-optimized and respectively subcloned into human IgG1 expression vectors, based on Gibson assembly, to generate recombinant mAbs. mAbs were produced by transient transfection into Expi293F cells with equal amounts of paired heavy- and light-chain expression vectors using the ExpiFectamine 293 transfection kit according to the manufacturer's protocol (Thermo Fisher). Five days post antibody expression, the secreted mAbs from cultured cells were collected and purified by affinity chromatography on rProtein A Sepharose Fast Flow beads according to the manufacturer's instructions (Cytiva). Eluted mAbs were further purified by size exclusion chromatography (SEC) using a Superdex 200 Increase 5/150 GL column (Cytiva), and the column was pre-equilibrated in 1x DPBS (Thermo). The purified mAbs were examined by running SDS-PAGE and kept in −80°C until needed.

### Omicron pseudovirus generation and neutralization assay

Omicron pseudovirus was generated by using a modified method from a previously described study. Briefly, a full-length Omicron spike gene was constructed into GFP encoding (pCCNanoLuc2AEGFP) human immunodeficiency vector backbone, then Omicron spike protein expression vectors were combined with HIV-1 structural corresponding plasmids and co-transfected into HEK-293T cells with PEI (1 mg/ml, PEI MAX, Polyscience). Two-day post-transfection, viral supernatants were harvested, collected, filtered, and aliquoted to use in assays.

Neutralization assays were performed by incubating pseudovirus with serial dilutions of mAbs. 10,000 cells/well of HEK-293T-hACE2 cells were seeded in a 96-well plate, 24 h before assay. mAbs supernatant/purified mAbs were serially diluted in DMEM media with 10% FBS and incubated with an equal volume of purified Omicron pseudovirus at 37°C for 1 h. Thereafter, the virus-antibody mixture was added in triplicate onto HEK-293T-hACE2 cells and grown at 37°C for an additional 24 h. Then, infected cells were counted and determined by evaluating GFP expression after 24 h of exposure to a virus-antibody mixture using Attune NxT Acoustic Focusing Cytometer (Thermo Fisher). Half-maximal inhibitory concentration (IC50) for mAbs was calculated with a four-parameter logistic regression using GraphPad Prism (GraphPad Software Inc.).

### Antibody binding kinetics, epitope mapping by bio-layer interferometry (BLI)

Antibody binding kinetics for anti-Omicron RBD mAbs were evaluated by BLI on an Octet RED96e instrument (FortéBio) at RT. 25 ng/ul of purified mAbs were captured on an AHC biosensor (Sartorius, 18–5060). The baseline was recorded for 60 s in a running buffer (PBS, 0.02% Tween 20, and 0.05% BSA, pH 7.4). Followed by sensors that were subjected to an association phase for 300 s in wells containing Omicron RBD with his tag protein diluted in the buffer. In the dissociation phase, the sensors were immersed in the running buffer for 500 s. The dissociation constants $K_D$, and kinetic constants $K_{on}$ and $K_{off}$ were calculated by FortéBio data analysis software.

For epitope mapping, two different antibodies were sequentially injected and monitored for binding activity to determine whether the two mAbs recognized separate or closely-situated epitopes by an in-tandem approach on OCTET RED. Briefly, SARS-CoV-2 RBD-His recombinant protein (Sino Biological 40,592-V08H121) was diluted with PBS to 20 μg/mL and was captured by anti-Penta-His (HIS1K) sensors (Sartorius, 18–5120). The primary antibody was diluted to 150 nM with running buffer in wells. Sensors were firstly subjected to an association phase for 500 s, and the response value was recorded. The sensors were then exposed to the secondary antibody mixture, and the response value was recorded again. Competition tolerance was calculated by the percentage increase in response after the secondary antibody was added. The column indicates the primary antibody, and the row indicates secondary antibodies. Competition tolerance of less than 25% indicates a high possibility of the closely-situated epitope.

### Antibody clone cellular binding testing

To validate binding ability of those top enriched IgG1/IgG2ab + clonotypes, paired heavy- and light-variable segments were cloned into human IgG1 expression vectors, transfected into the Expi293F cell mammalian expression system to produce individual clones

of mAbs. Target overexpression cells (e.g. Omicron S in HEK293 cells, GPRC5D in K562 cells) were generated either by lentiviral cDNA expression, or by transfection or electroporation of respective mRNAs. Transfected culture supernatants that contain secreted antibodies were used as primary Ab in cell staining assay to determine antibody binding on cell surface of target overexpression cells. For flow staining, 200 μL of each transfected culture supernatant that contains secreted antibodies was co-cultured with target over-expressed cells for 1 h at 4°C. Thereafter, the cells were washed twice with MACS buffer, then incubated with anti-hIgG-PE antibodies for additional 30 min on ice. The binding activity was determined using flow cytometry.

### Chemical compounds

No original chemical compounds such as small molecule or peptide were generated. Standard chemical compounds had been sourced from commercial vendors as described in method details. For biomolecules such as antibody constructs, identity is based on sequence and the constructs are sequence verified.

### Oligo sequences

Oligo sequences related to this study are provided in Table S3.

## QUANTIFICATION AND STATISTICAL ANALYSIS

### Standard statistics

Standard statistical methods were applied to non-high-throughput experimental data. Prism (GraphPad Software) and RStudio were used for these analyses. The statistical significance was labeled as follows: n.s., not significant; *$p < 0.05$; **$p < 0.01$; ***$p < 0.001$; ****$p < 0.0001$. The source data, statistical analyses, statistical details of experiments can be found in figure legends and/or supplementary Excel tables. Additional information can be found in the supplemental excel tables.

### Schematic illustrations

Schematic illustrations were created with Affinity Designer or BioRender.

### Replication, randomization, blinding and reagent validations

Sample size: Sample size determination was performed according to similar work in the field.

Replicate experiments have been performed for key data shown in this study.

Replication: Biological or technical replicate samples were randomized where appropriate. In animal experiments, mice were randomized by cage, sex and littermates.

Binding: Experiments were not blinded. It is unnecessary for animal immunization for antibody production to be blinded.

Antibodies and dilutions: Commercial antibodies used for various experiments are described in methods, with typical dilutions noted. For custom Antibodies generated in this study, dilutions were often serial titrations (i.e. a number of dilutions as specified in each figure). Commercial antibodies were validated by the vendors, and re-validated in house as appropriate. Custom antibodies were validated by specific antibody-antigen interaction assays, such as ELISA. isotype controls were used for antibody validations.

Eukaryotic cell lines: Cell lines are from various sources as described in methods. Cell lines were authenticated by original vendors, and re-validated in lab as appropriate. All cell lines tested negative for mycoplasma. No commonly misidentified lines involved.

Animals and other organisms: Laboratory animals: *M. musculus*, ATX strain (Alloy Tx).

## ADDITIONAL RESOURCES

Information on additional resources relevant to this study is provided at KRT.